

# Type II band alignment of NiO/ $\alpha$ -Ga<sub>2</sub>O<sub>3</sub> for annealing temperatures up to 600 °C

Cite as: J. Vac. Sci. Technol. A **40**, 063408 (2022); <https://doi.org/10.1116/6.0002257>

Submitted: 29 September 2022 • Accepted: 31 October 2022 • Published Online: 15 November 2022

 Xinyi Xia, Jian-Sian Li,  Chao-Ching Chiang, et al.

## COLLECTIONS

Paper published as part of the special topic on [Gallium Oxide Materials and Devices](#)



[View Online](#)



[Export Citation](#)



[CrossMark](#)

## ARTICLES YOU MAY BE INTERESTED IN

[A review of Ga<sub>2</sub>O<sub>3</sub> materials, processing, and devices](#)

Applied Physics Reviews **5**, 011301 (2018); <https://doi.org/10.1063/1.5006941>


[Critical review of Ohmic and Schottky contacts to  \$\beta\$ -Ga<sub>2</sub>O<sub>3</sub>](#)

Journal of Vacuum Science & Technology A **40**, 060802 (2022); <https://doi.org/10.1116/6.0002144>


[\$\beta\$ -Gallium oxide power electronics](#)

APL Materials **10**, 029201 (2022); <https://doi.org/10.1063/5.0060327>









**HIDEN**  
ANALYTICAL



40 YEARS  
1982 - 2022

## Instruments for Advanced Science

<p>■ Knowledge, ■ Experience, ■ Expertise</p> <p style="background-color: #c00000; color: white; text-align: center; padding: 2px;">Click to view our product catalogue</p> <p>Contact Hiden Analytical for further details:  <a href="http://www.HidenAnalytical.com">www.HidenAnalytical.com</a>  <a href="mailto:info@hideninc.com">info@hideninc.com</a></p>	<p style="background-color: #c00000; color: white; text-align: center; padding: 2px;"><b>Gas Analysis</b></p>  <ul style="list-style-type: none"> <li>▶ dynamic measurement of reaction gas streams</li> <li>▶ catalysis and thermal analysis</li> <li>▶ molecular beam studies</li> <li>▶ dissolved species probes</li> <li>▶ fermentation, environmental and ecological studies</li> </ul>	<p style="background-color: #c00000; color: white; text-align: center; padding: 2px;"><b>Surface Science</b></p>  <ul style="list-style-type: none"> <li>▶ UHV-TPD</li> <li>▶ SIMS</li> <li>▶ end point detection in ion beam etch</li> <li>▶ elemental imaging - surface mapping</li> </ul>	<p style="background-color: #c00000; color: white; text-align: center; padding: 2px;"><b>Plasma Diagnostics</b></p>  <ul style="list-style-type: none"> <li>▶ plasma source characterization</li> <li>▶ etch and deposition process reaction kinetic studies</li> <li>▶ analysis of neutral and radical species</li> </ul>
<p style="background-color: #c00000; color: white; text-align: center; padding: 2px;"><b>Vacuum Analysis</b></p>  <ul style="list-style-type: none"> <li>▶ partial pressure measurement and control of process gases</li> <li>▶ reactive sputter process control</li> <li>▶ vacuum diagnostics</li> <li>▶ vacuum coating process monitoring</li> </ul>			

# Type II band alignment of NiO/ $\alpha$ -Ga<sub>2</sub>O<sub>3</sub> for annealing temperatures up to 600 °C

Cite as: J. Vac. Sci. Technol. A 40, 063408 (2022); doi: 10.1116/6.0002257

Submitted: 29 September 2022 · Accepted: 31 October 2022 ·

Published Online: 15 November 2022



Xinyi Xia,<sup>1</sup> Jian-Sian Li,<sup>1</sup> Chao-Ching Chiang,<sup>1</sup> Timothy Jinsoo Yoo,<sup>2</sup> Eitan HersHKovitz,<sup>2</sup> Fan Ren,<sup>1</sup> Honggyu Kim,<sup>2</sup> Jihyun Kim,<sup>3</sup> Dae-Woo Jeon,<sup>4</sup> Ji-Hyeon Park,<sup>4</sup> and S. J. Pearton<sup>2,a)</sup>

## AFFILIATIONS

<sup>1</sup>Department of Chemical Engineering, University of Florida, Gainesville, Florida 32606

<sup>2</sup>Department of Materials Science and Engineering, University of Florida, Gainesville, Florida 32606

<sup>3</sup>School of Chemical and Biological Engineering, Seoul National University, Seoul 08826, South Korea

<sup>4</sup>Korea Institute of Ceramic Engineering and Technology, Jinju 52851, South Korea

**Note:** This paper is part of the Special Topic Collection on Gallium Oxide Materials and Devices.

**a) Author to whom correspondence should be addressed:** [spear@mse.ufl.edu](mailto:spear@mse.ufl.edu)

## ABSTRACT

There is increasing interest in the alpha polytype of Ga<sub>2</sub>O<sub>3</sub> because of its even larger bandgap than the more studied beta polytype, but in common with the latter, there is no viable p-type doping technology. One option is to use p-type oxides to realize heterojunctions and NiO is one of the candidate oxides. The band alignment of sputtered NiO on  $\alpha$ -Ga<sub>2</sub>O<sub>3</sub> remains type II, staggered gap for annealing temperatures up to 600 °C, showing that this is a viable approach for hole injection in power electronic devices based on the alpha polytype of Ga<sub>2</sub>O<sub>3</sub>. The magnitude of both the conduction and valence band offsets increases with temperature up to 500 °C, but then is stable to 600 °C. For the as-deposited NiO/ $\alpha$ -Ga<sub>2</sub>O<sub>3</sub> heterojunction,  $\Delta E_V = -2.8$  and  $\Delta E_C = 1.6$  eV, while after 600 °C annealing the corresponding values are  $\Delta E_V = -4.4$  and  $\Delta E_C = 3.02$  eV. These values are 1–2 eV larger than for the NiO/ $\beta$ -Ga<sub>2</sub>O<sub>3</sub> heterojunction.

Published under an exclusive license by the AVS. <https://doi.org/10.1116/6.0002257>

## I. INTRODUCTION

The thermodynamically stable form of Ga<sub>2</sub>O<sub>3</sub> is the monoclinic  $\beta$ -phase (C2/m), but there are at least five other phases identified. The monoclinic  $\beta$ - polymorph has attracted the most attention of the six different polymorphs of Ga<sub>2</sub>O<sub>3</sub>, but there is increasing interest in metastable corundum  $\alpha$ -Ga<sub>2</sub>O<sub>3</sub> due to its even larger bandgap and compatibility with growth on isomorphous sapphire ( $\alpha$ -Al<sub>2</sub>O<sub>3</sub>) substrates.<sup>1–25</sup> The corundum  $\alpha$ -Ga<sub>2</sub>O<sub>3</sub> belongs to the trigonal R3c space group ( $a = 5.059\,52\,\text{\AA}$ ,  $c = 13.624\,80\,\text{\AA}$ ,  $\alpha = \beta = \gamma = 120^\circ$ ).<sup>3–5</sup> This highly asymmetric monoclinic structure leads to anisotropic materials properties and challenges in crystal growth, leading to more attention on the  $\alpha$ -polytype, which has higher symmetry and more facile epitaxial growth conditions than  $\beta$ -Ga<sub>2</sub>O<sub>3</sub>.<sup>1–5</sup> It is known that epitaxial films of  $\alpha$ -polytype Ga<sub>2</sub>O<sub>3</sub> grown on m-plane sapphire are stable up to 600 °C anneal temperatures but are metastable and converts to the  $\beta$ -phase after annealing at 800 °C,<sup>26</sup> but this allows a practical window for device processing and many reports of alpha-polytype devices exist.

To overcome the absence of conventional p-type dopants for  $\alpha$ -Ga<sub>2</sub>O<sub>3</sub> and be able to realize p-n junction devices, a variety of p-type oxides have been integrated with n-type Ga<sub>2</sub>O<sub>3</sub>. For the alpha polytype, these have included Ir<sub>2</sub>O<sub>3</sub>, which can be lattice-matched to  $\alpha$ -Ga<sub>2</sub>O<sub>3</sub>.<sup>27</sup> The band alignment of the  $\alpha$ -Ga<sub>2</sub>O<sub>3</sub>/a-Ir<sub>2</sub>O<sub>3</sub> heterojunction is a staggered gap, type-II, with valence- and conduction-band offsets of 3.34 and 1.04 eV, respectively.<sup>28</sup> Similarly, the band alignment of atomic layer-deposited BeO and  $\beta$ -Ga<sub>2</sub>O<sub>3</sub> has been reported.<sup>28</sup> However, for hole injection purposes, it is not necessary to have a lattice-matched layer and more common alternatives such as NiO can be considered for devices such as vertical p–n heterojunction rectifiers.<sup>29–33</sup> Several previous studies reported that NiO has a staggered type II alignment on  $\beta$ -Ga<sub>2</sub>O<sub>3</sub>, allowing for efficient hole injection.<sup>29–33</sup> However, to date, there has been no measurement of band alignments of NiO on the other polytypes of Ga<sub>2</sub>O<sub>3</sub> and especially this is important for the alpha polytype due to its large bandgap and exceptional promise for power devices with high figures-of-merit.

In this paper, we carry out a similar study for NiO on  $\alpha$ -Ga<sub>2</sub>O<sub>3</sub> and establish that there is also a type II alignment, and this remains the case up to annealing temperatures of 600 °C. This is important since it covers the thermal budget of most common device processing steps and establishes NiO as a potential p-type oxide for heterojunction power devices based on  $\alpha$ -Ga<sub>2</sub>O<sub>3</sub>. The thermal stability of NiO/ $\alpha$ -Ga<sub>2</sub>O<sub>3</sub> heterointerfaces is also of interest from comparing with conventional metal contacts used for Schottky rectifiers since this is also a factor in their potential device applications.

## II. EXPERIMENT

The  $\alpha$ -Ga<sub>2</sub>O<sub>3</sub> layers were grown by hydride vapor phase epitaxy on (0001) sapphire substrates. The growth temperature was 470 °C.<sup>34</sup> The gaseous precursors were HCl and O<sub>2</sub>. Pure Ga metal was used to form GaCl and GaCl<sub>3</sub> as precursors for Ga<sub>2</sub>O<sub>3</sub>. These gases were transported to the reactor using N<sub>2</sub> carrier gas. The thicknesses of the  $\alpha$ -Ga<sub>2</sub>O<sub>3</sub> epilayers were 1.2  $\mu$ m, at a growth rate of  $\sim$ 6  $\mu$ m/h, or growth times of the order of 10 min.

The properties of NiO depend on controlling the stoichiometry during deposition for as-deposited films. Our films were 6–60 nm thick and deposited by magnetron sputtering at 3 mTorr and 150 W of 13.56 MHz power using two targets to achieve a deposition rate around 0.2 Å s<sup>−1</sup>. For calibration experiments, the depositions were performed onto quartz substrates. Since the depositions were done at room temperature where the surface mobility is small, it is not expected that there will be much difference in the structure of the NiO deposited on quartz or Ga<sub>2</sub>O<sub>3</sub>. This was done to avoid complications from possible defect-related absorption in the Ga<sub>2</sub>O<sub>3</sub>. The Ar/O<sub>2</sub> ratio during sputtering was used to control the doping in NiO at  $5 \times 10^{18}$  cm<sup>−3</sup>, with hole mobility  $< 1$  cm<sup>2</sup> V<sup>−1</sup> s<sup>−1</sup>. The temperature of the sample during deposition was  $< 100$  °C. The bandgaps were determined for as-deposited and annealed films using UV-Vis (Perkin-Elmer Lambda 800 UV/Vis spectrometer). The absorbance spectrum was collected and Tauc plots were used to calculate the bandgap of the NiO. As summarized in a recent review,<sup>35</sup> conflicting previous reports have interpreted the bandgap as either direct<sup>36</sup> or indirect.<sup>37</sup> Since band structure calculations show the presence of both,<sup>35</sup> we calculated the values for both using the usual power law,  $(\alpha h\nu)^n = C(h\nu - E_g)$ , where  $\alpha$  is the absorption coefficient,  $h\nu$  is the photon energy,  $E_g$  is the bandgap, and  $C$  is a constant. For indirect bandgaps, the exponent  $n$  is 0.5, while for direct gaps it is 2.<sup>38,39</sup> The extrapolation of a linear fit on these respective Tauc plots provides the bandgap.<sup>39</sup> As will be seen, we found better fits for the assumption of a direct gap.

The band alignments were determined from the standard x-ray photoelectron spectroscopy (XPS) method,<sup>40–43</sup> in which the core levels and valence band maxima (VBM) positions are measured from a thick (60 nm) NiO layer and in the epitaxial  $\alpha$ -Ga<sub>2</sub>O<sub>3</sub>. These same core level locations were re-measured in a NiO/ $\alpha$ -Ga<sub>2</sub>O<sub>3</sub> heterojunction consisting of 6 nm NiO sputtered on  $\alpha$ -Ga<sub>2</sub>O<sub>3</sub>. The shift of the core level binding energy locations ( $\Delta E_{CL}$ ) within the heterostructure determines the valence band offset ( $\Delta E_V$ ) from<sup>44,45</sup>

$$\Delta E_V = \Delta E_{CL} + (E_{Core} - E_{VBM})_{Ref. NiO} - (E_{Core} - E_{VBM})_{Ref. Ga_2O_3}$$

The XPS system has been described in detail previously,<sup>29,44,45</sup> but in brief is a Physical Instruments ULVAC PHI, with an Al x-ray source (energy 1486.6 eV, source power 300 W), an analysis size of 100  $\mu$ m diameter, a take-off angle of 50°, and an acceptance angle of  $\pm 7^\circ$ . The electron pass energy was 23.5 eV for high-resolution scans. The total energy resolution of this XPS system is about 0.5 eV, and the accuracy of the observed binding energy is within 0.03 eV. When applied correctly,<sup>41–43</sup> the XPS method is a reliable one for determining band offsets and avoids issues of the influence of defects states on alternative current or capacitance-based methods.

For high-angle annular dark-field (HAADF) imaging in scanning transmission electron microscopy (STEM), cross section microscopy samples of a 300 °C annealed NiO/ $\alpha$ -Ga<sub>2</sub>O<sub>3</sub> heterostructure were prepared along the  $[\bar{1}000]$  zone axis of  $\alpha$ -Ga<sub>2</sub>O<sub>3</sub> using a FEI Helios Dual Beam Nanolab 600 focused ion beam (FIB) system. HAADF-STEM imaging of the NiO/ $\alpha$ -Ga<sub>2</sub>O<sub>3</sub> interface structure was carried out using a 200 kV Themis Z (Thermo Scientific) equipped with a probe aberration corrector and a HAADF detector with an inner collection angle of 58 mrad.

## III. RESULTS AND DISCUSSION

Figure 1 shows the HAADF-STEM imaging results for a 300 °C annealed NiO/ $\alpha$ -Ga<sub>2</sub>O<sub>3</sub> heterostructure. Figure 1(a) is a HAADF-STEM image of the full diode structure, consisting of the top p-type NiO and bottom n-type  $\alpha$ -Ga<sub>2</sub>O<sub>3</sub>, recorded along the

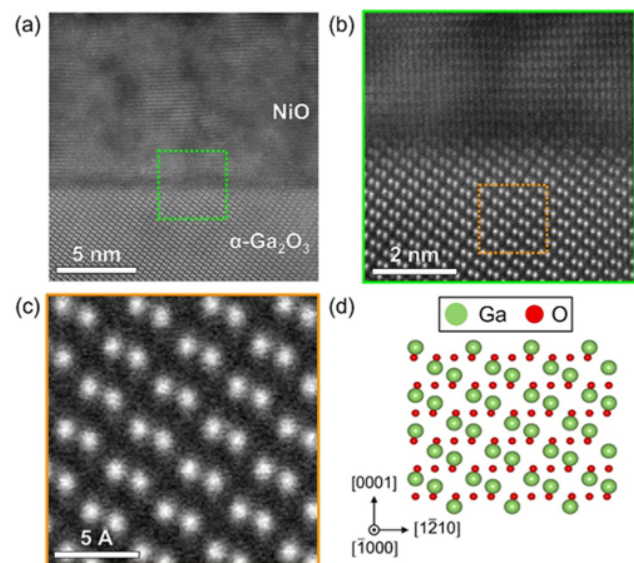


**FIG. 1.** (a) HAADF-STEM image of NiO/ $\alpha$ -Ga<sub>2</sub>O<sub>3</sub> heterostructure. (b) High magnification HAADF-STEM image from the dashed green box in (a) showing that the interface between NiO/ $\alpha$ -Ga<sub>2</sub>O<sub>3</sub> is atomically sharp. (c) HAADF-STEM image and (d) schematic of the atomic structure of  $\alpha$ -Ga<sub>2</sub>O<sub>3</sub> outlined in the dashed orange box in (b) revealing the  $[1000]$  zone axis and the (0001) growth surface of  $\alpha$ -Ga<sub>2</sub>O<sub>3</sub>. Ga atoms are the larger ones (green) while O atoms are small (red).

[ $\bar{1}000$ ] projection with respect to the trigonal  $\alpha$ -Ga<sub>2</sub>O<sub>3</sub>. The high magnification HAADF-STEM image in Fig. 1(b) reveals that the NiO/ $\alpha$ -Ga<sub>2</sub>O<sub>3</sub> interface is atomically abrupt and that  $\alpha$ -Ga<sub>2</sub>O<sub>3</sub> near the heterointerface is pristine without extended defects. The annealing strategy employed in this study is shown to be effective at relieving previously observed, sputtering-induced damage at the interface.<sup>46</sup> Figures 1(c) and 1(d) are a high magnification HAADF-STEM image and schematic of the  $\alpha$ -Ga<sub>2</sub>O<sub>3</sub> atomic structure viewed along [ $\bar{1}000$ ], demonstrating that the growth plane of the  $\alpha$ -Ga<sub>2</sub>O<sub>3</sub> film is (0001). Note that due to the relatively low atomic number of oxygen ( $Z = 8$ ) as compared to Ga ( $Z = 31$ ), only Ga atomic columns are visible in HAADF-STEM images.

The valence band offsets were obtained from the XPS core level shifts in the heterostructure samples, while the bandgaps of the NiO and  $\alpha$ -Ga<sub>2</sub>O<sub>3</sub> were obtained from Tauc plots and XPS and core-valence band maxima (VBM) measurements, respectively. Knowing both the bandgaps and valence band offsets, then allowed the calculation of the conduction-band offsets. This was done for separate layers of NiO annealed for 5 min at temperatures from 300 to 600 °C under an O<sub>2</sub> ambient using rapid thermal annealing. We kept the annealing ambient constant and chose O<sub>2</sub> to avoid possibly creating oxygen vacancies, which are known to strongly influence the electrical properties of many oxides. Figure 2(a) shows Ultraviolet-Visible Spectroscopy (UV-Vis) absorption data, while the corresponding Tauc plots are shown in Fig. 2(b) for power law of 2 (direct gap) and in Fig. 2(c) for a power law of 0.5 (indirect gap). There is a better fit for the former. The extracted direct bandgap decreased with annealing temperature, from 3.90 eV for as-deposited films to 3.72 eV for those annealed at 600 °C, as tabulated in Table I. For completeness, we also include the results extracted if the gap is indirect and where there was a reasonable straight section of the plot to extrapolate from, with the values being  $\sim 0.5$  eV smaller than the direct gaps. The bandgap of the as-deposited NiO and the small changes with annealing are consistent with the range of values reported in the literature.<sup>36</sup> Changes with annealing could be due to the fact that with increasing annealing temperature, more oxygen escapes from the film, corresponding to a decrease in the Ni<sub>2</sub>O<sub>3</sub>/NiO ratio. With an increase in annealing temperature, the bandgap decreases due to more NiO being formed relative to Ni<sub>2</sub>O<sub>3</sub>.

The bandgap of  $\alpha$ -Ga<sub>2</sub>O<sub>3</sub> was determined using the onset of the plasmon loss feature in O 1s photoemission spectrum, as shown in Fig. 3(a). The XPS spectra of core levels to valence band maximum for  $\alpha$ -Ga<sub>2</sub>O<sub>3</sub> are shown in Fig. 3(b) and the values are also tabulated in Table I. Our value for the bandgap is within the reported ranges for  $\alpha$ -Ga<sub>2</sub>O<sub>3</sub>.<sup>1,35</sup> We did not calculate the bandgap of  $\alpha$ -Ga<sub>2</sub>O<sub>3</sub> using a Tauc plot, because this method is less accurate for large bandgap materials, and thus we preferred the onset of the plasmon loss feature in O 1s photoemission spectrum. The  $\alpha$ -Ga<sub>2</sub>O<sub>3</sub> bandgap was independent of annealing temperature.

The high-resolution XPS spectra for the vacuum-core delta regions of Ga<sub>2</sub>O<sub>3</sub> are shown in Fig. 4 for heterojunction samples annealed at different temperatures up to 600 °C. The  $\Delta E_V$  values are then extracted from the shift of the core levels for the heterojunction samples with the thin NiO overlayers.<sup>38,39</sup> The XPS spectrum indicated that nickel was in the 2+ oxidation state in NiO. We used the Kraut method described earlier to measure the

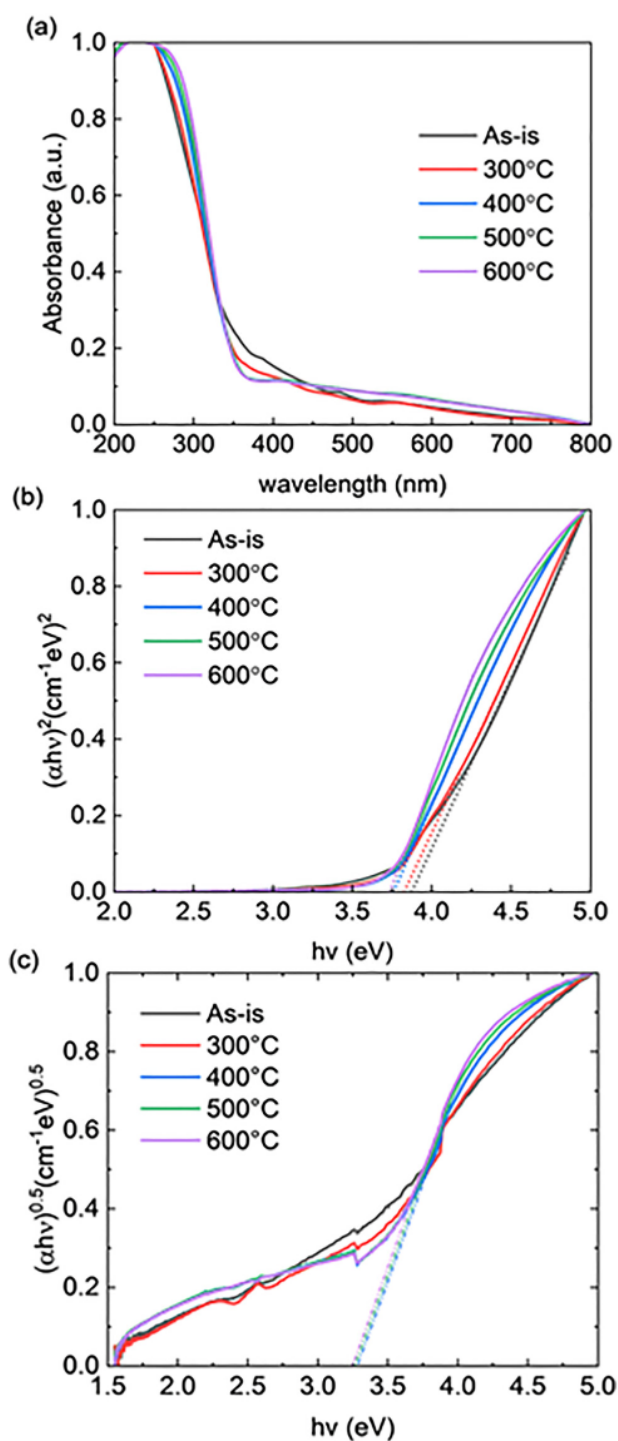


**FIG. 2.** (a) NiO absorbance spectrum measured by UV-vis. Tauc plot for the extrapolation of (b) direct bandgaps of NiO and (c) indirect bandgaps of NiO as-is and annealed at different temperatures.



**TABLE I.** (Top) NiO bandgap measured by UV-vis and fitting to either direct or indirect bandgap. (Bottom) Valence band maximum and core level data used to calculate the bandgap of  $\alpha$ -Ga<sub>2</sub>O<sub>3</sub>.

	As-is	300 °C	400 °C	500 °C	600 °C
Direct energy bandgap (eV)	3.90	3.84	3.76	3.74	3.72
Indirect energy bandgap (eV)	N/A	N/A	3.28	3.26	3.25
$\alpha$ -Ga <sub>2</sub> O <sub>3</sub>					
VBM	Core level peak (Ga2p <sub>3/2</sub> )		Core-VBM		Bandgap (eV)
3.5	1117.1		1113.6		5.1

valence band offsets by observing the shift of the core levels from  $\alpha$ -Ga<sub>2</sub>O<sub>3</sub> when NiO was deposited. The XPS spectra from which we extracted the core energy differences to VBM for thick NiO layers after different annealing temperatures are shown in Fig. 5. The valence band maxima values were determined by linear extrapolation of the leading edge to the baseline of the valence band spectra. The corresponding VBMs are shown in Table II. The error

bars in the different binding energies were combined in a root sum square relationship to determine the overall error bars in the valence band offsets.<sup>33</sup> Note that sample charging is not an issue when determining band offsets since we only need peak core shift

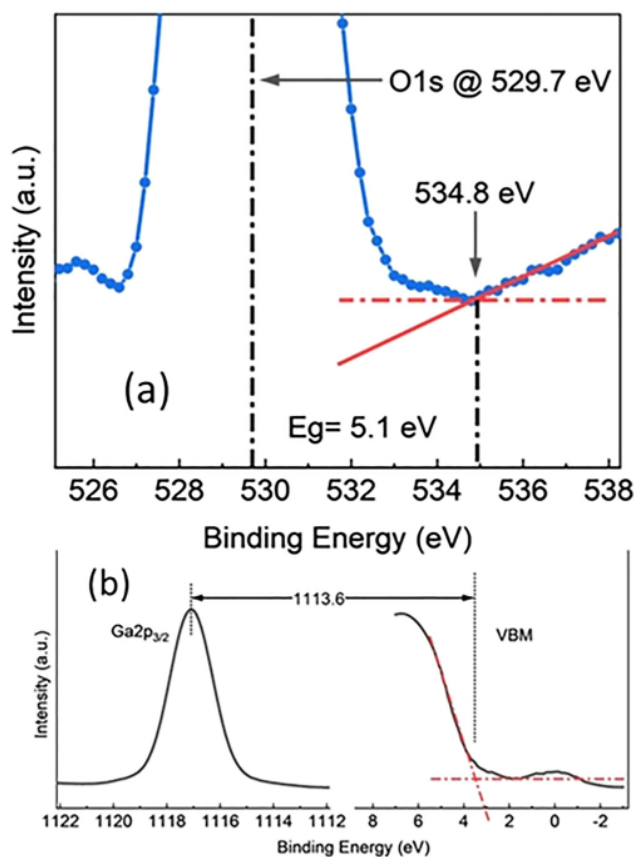


**FIG. 3.** (a) Bandgap of  $\alpha$ -Ga<sub>2</sub>O<sub>3</sub> determined using the onset of the plasmon loss feature in O 1s photoemission spectrum. (b) XPS spectra of core levels to valence band maximum for  $\alpha$ -Ga<sub>2</sub>O<sub>3</sub>.

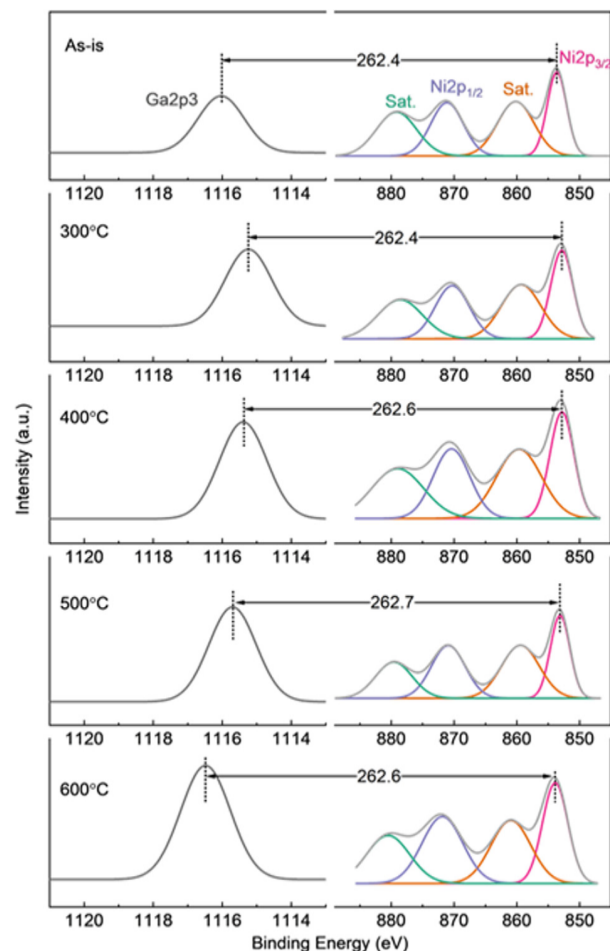


**FIG. 4.**  $\Delta$  Core level energies for interfaces of thin NiO/ $\alpha$ -Ga<sub>2</sub>O<sub>3</sub> as-is and annealed at different temperatures.

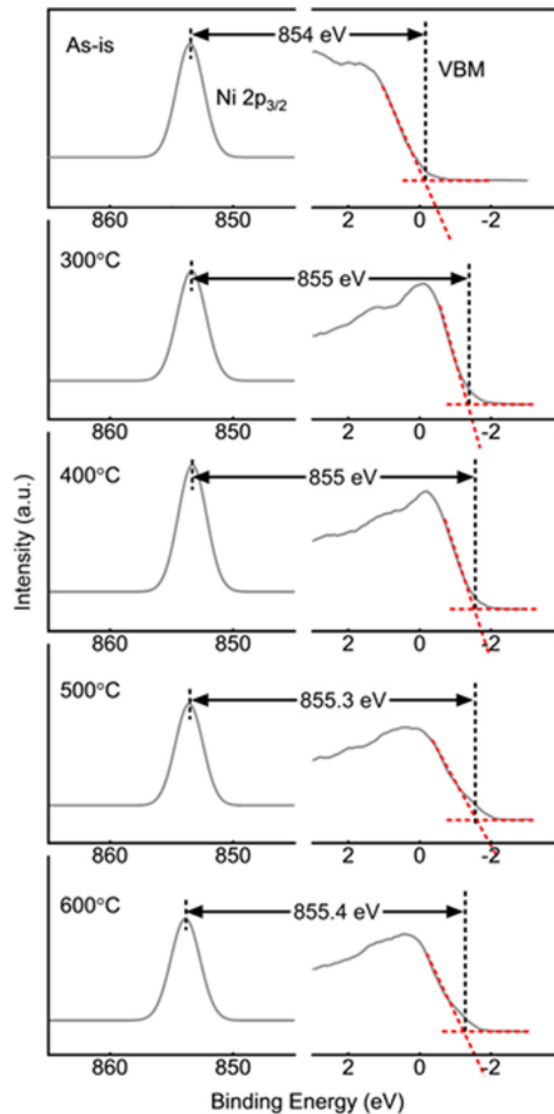


**FIG. 5.** Core-VBM energies for thick NiO film as-deposited and annealed at different temperatures.

deltas, which will shift all binding energies by the same amount. We also did not observe any differential charging, which could shift peaks by different amounts and could potentially be a large source of error.

Figure 6 shows the band alignment of NiO on  $\alpha$ -Ga<sub>2</sub>O<sub>3</sub> after the different annealing temperatures. Note that there is a staggered type II alignment across the entire annealing range investigated, which is advantageous for hole injection. The valence band offsets were  $2.8 \pm 0.30$  eV for the as-deposited heterojunction,  $3.8 \pm 0.35$  eV after annealing at 300 °C,  $4.0 \pm 0.35$  eV after annealing at 400 °C, and  $4.4 \pm 0.4$  eV for annealing at 500 and at 600 °C. The respective conduction-band offsets vary from 1.6 to 3.04 eV. Note that the band offsets increase monotonically with annealing temperature and will not provide any barrier to electrons moving into the Ga<sub>2</sub>O, suggesting that NiO may not work as an effective guard-ring material on  $\alpha$ -Ga<sub>2</sub>O<sub>3</sub> rectifiers. Thus, it would be necessary to have separate electrode materials for hole injection (NiO) and mitigation of peak electric fields. Standard metals such as Au or Ni might be superior choices for the guard-ring fabrication.<sup>47</sup> While both vertical Schottky rectifiers and heterojunction diodes with Rh<sub>2</sub>O<sub>3</sub>,<sup>48</sup> Ir<sub>2</sub>O<sub>3</sub>,<sup>24,25</sup> or (Ir<sub>x</sub>Ga<sub>1-x</sub>)<sub>2</sub>O<sub>3</sub><sup>49,50</sup> based on  $\alpha$ -Ga<sub>2</sub>O<sub>3</sub> have been reported, there has been little development of edge termination methods for alpha-polytype devices.<sup>47</sup>

It is also important to note that the band alignment results were independent of the NiO thickness over the range we examined, which was 3–7 nm. Of course, this is limited by the need to probe through the layer to measure the core levels in the underlying Ga<sub>2</sub>O<sub>3</sub>.

While annealing a sputtered material may change its crystallinity, preliminary STEM measurements on the NiO did not show significant structural changes with annealing, and it is difficult to quantify interfacial changes due to both materials being oxides so that the diffusion of oxygen cannot be quantified. However, this does suggest that changes in point defect population play a strong role in the changes in band alignment. This is reflected in the changes in bandgap of the NiO with annealing. The crystallinity and defect and carrier concentrations under different annealing temperatures could also play an important role in determining the band alignments, as in the  $\alpha$ -Ga<sub>2</sub>O<sub>3</sub>/a-Ir<sub>2</sub>O<sub>3</sub> heterojunction.<sup>29</sup> However, such a study is beyond the scope of the current work, which focusses on the XPS results and some TEM after 300 °C annealing. Future work will focus on the structural and electrical changes in the NiO under different annealing temperatures.

**TABLE II.** Core level data measured by XPS data as a function of postdeposition annealing temperature.

	Reference NiO			Thin NiO on $\alpha$ -Ga <sub>2</sub> O <sub>3</sub>			
	VBM	Core level peak (Ni 2p <sub>3/2</sub> )	Core-VBM	Core level peak (Ga 2p <sub>3/2</sub> )	Core level peak (Ni 2p <sub>3/2</sub> )	$\Delta$ Core level	Valence band offset
As-is	-0.6	853.4	854	1116	853.6	262.4	2.8
300 °C	-1.8	853.2	855	1115.2	852.8	262.4	3.8
400 °C	-1.9	853.1	855	1115.4	852.8	262.6	4
500 °C	-1.9	853.4	855.3	1115.7	853	262.7	4.4
600 °C	-1.7	853.7	855.4	1116.4	853.8	262.6	4.4

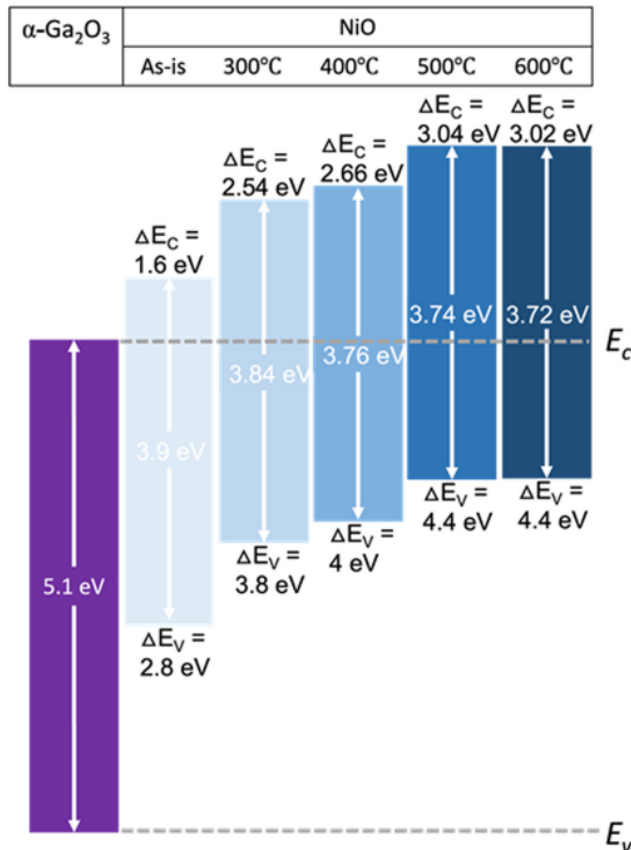


**FIG. 6.** Schematic of band alignments for NiO/ $\alpha$ -Ga<sub>2</sub>O<sub>3</sub> as a function of postdeposition annealing temperature.

#### IV. SUMMARY AND CONCLUSIONS

The band alignment of NiO/ $\alpha$ -Ga<sub>2</sub>O<sub>3</sub> interfaces and how this varies with annealing temperature has been determined and shows potential for realizing p-n junction power devices based on the alpha polytype of Ga<sub>2</sub>O<sub>3</sub>. The type II staggered alignment is retained up to 600 °C, which is a practical thermal budget for fabrication of power rectifiers. The results for the NiO on  $\alpha$ -Ga<sub>2</sub>O<sub>3</sub> show the same general trends as for the same heterojunction on  $\beta$ -Ga<sub>2</sub>O<sub>3</sub>, but an added issue with the former is the limited thermal stability of the alpha polytype. IrO<sub>x</sub> also has a staggered gap, type-II alignment with  $\alpha$ -Ga<sub>2</sub>O<sub>3</sub> with valence- and conduction-band offsets of 3.34 and 1.04 eV, respectively, of the same general magnitude as NiO. It will be interesting to see valence band offsets for other p-type oxides on  $\alpha$ -Ga<sub>2</sub>O<sub>3</sub>.

#### ACKNOWLEDGMENTS

The work at University of Florida (UF) was performed as part of Interaction of Ionizing Radiation with Matter University Research Alliance (IIRM-URA), sponsored by the Department of

the Defense, Defense Threat Reduction Agency under Award No. HDTRA1-20-2-0002. The content of the information does not necessarily reflect the position or the policy of the federal government, and no official endorsement should be inferred. The work at UF was also supported by National Science Foundation Division of Materials Research under No. 1856662 (James Edgar). The work in Korea was supported by the Korea Institute for Advancement of Technology (KIAT) grant (No. P0012451, The Competency Development Program for Industry Specialist), the Institute of Civil Military Technology Cooperation Center funded by the Defense Acquisition Program Administration and MOTIE, and of Korean Government under Grant No. 20-CM-BR-05 and the National Research Foundation of Korea (NRF) grant funded by the Korea Government (MSIT) (No. 2020M3H4A3081796).

#### AUTHOR DECLARATIONS

##### Conflict of Interest

The authors have no conflicts to disclose.

#### Author Contributions

**Xinyi Xia:** Conceptualization (equal); Data curation (equal); Formal analysis (equal); Writing – original draft (equal). **Jian-Sian Li:** Conceptualization (equal); Formal analysis (equal); Writing – original draft (equal). **Chao-Ching Chiang:** Conceptualization (equal); Data curation (equal); Writing – original draft (equal). **Timothy Jinsoo Yoo:** Conceptualization (equal); Data curation (equal); Formal analysis (equal); Writing – original draft (equal). **Eitan HersHKovitz:** Conceptualization (equal); Data curation (equal). **Fan Ren:** Conceptualization (equal); Formal analysis (equal); Funding acquisition (equal); Writing – original draft (equal). **Honggyu Kim:** Conceptualization (equal); Data curation (equal); Formal analysis (equal); Writing – original draft (equal). **Jihyun Kim:** Conceptualization (equal); Data curation (equal); Funding acquisition (equal); Writing – original draft (equal). **Dae-Woo Jeon:** Conceptualization (equal); Data curation (equal); Writing – original draft (equal). **Ji-Hyeon Park:** Conceptualization (equal); Data curation (equal); Writing – original draft (equal). **S. J. Pearton:** Conceptualization (equal); Data curation (equal); Writing – original draft (equal).

#### DATA AVAILABILITY

The data that support the findings of this study are included within the article.

#### REFERENCES

- <sup>1</sup>D. E. Ahmadi and Y. Oshima, *J. Appl. Phys.* **126**, 160901 (2019).
- <sup>2</sup>T. Maeda, M. Okigawa, Y. Kato, I. Takahashi, and T. Shinohe, *AIP Adv.* **10**, 125119 (2020).
- <sup>3</sup>A. Hassa, P. Storm, M. Kneiß, D. Splith, H. von Wenckstern, M. Lorenz, and M. Grundmann, *Phys. Status Solidi B* **258**, 2000394 (2021).
- <sup>4</sup>H. Zhang, L. Yuan, X. Tang, J. Hu, J. Sun, Y. Zhang, Y. Zhang, and R. Jia, *IEEE T. Power Electr.* **35**, 5157 (2020).
- <sup>5</sup>A. Y. Polyakov, V. I. Nikolaev, E. B. Yakimov, F. Ren, S. J. Pearton, and J. Kim, *J. Vac. Sci. Technol. A* **40**, 020804 (2022).

- <sup>6</sup>Z. Wang, X. Chen, F.-F. Ren, S. Gu, and J. Ye, *J. Phys D: Appl. Phys.* **54**, 043002 (2021).
- <sup>7</sup>C. Cora, Z. Fogarassy, R. Fornari, M. Bosi, A. Rečnik, and B. Pecz, *Acta Mater.* **183**, 216 (2020).
- <sup>8</sup>A. F. M. A. U. Bhuiyan *et al.*, *APL Mater.* **8**, 031104 (2020).
- <sup>9</sup>M. Hilfiker, U. Kilic, M. Stokey, R. Jinno, Y. Cho, H. G. Xing, D. Jena, R. Korlacki, and M. Schubert, *Appl. Phys. Lett.* **119**, 092103 (2021).
- <sup>10</sup>K. Uno, R. Jinno, and S. Fujita, *J. Appl. Phys.* **131**, 090902 (2022).
- <sup>11</sup>J. A. Spencer, A. L. Mock, A. G. Jacobs, M. Schubert, Y. Zhang, and M. J. Tadjer, *Appl. Phys. Rev.* **9**, 011315 (2022).
- <sup>12</sup>D. Yang, B. Kim, T. H. Eom, Y. Park, and H. W. Jang, *Electron. Mater. Lett.* **18**, 113 (2022).
- <sup>13</sup>R. Schewski *et al.*, *Appl. Phys. Express* **8**, 011101 (2015).
- <sup>14</sup>M. Kracht, A. Karg, M. Feneberg, J. Bläsing, J. Schörmann, R. Goldhahn, and M. Eickhoff, *Phys. Rev. Appl.* **10**, 024047 (2018).
- <sup>15</sup>Y. Oshima, K. Kawara, T. Shinohe, T. Hitora, M. Kasu, and S. Fujita, *APL Mater.* **7**, 022503 (2019).
- <sup>16</sup>K. Kawara, Y. Oshima, M. Okigawa, and T. Shinohe, *Appl. Phys. Express* **13**, 075507 (2020).
- <sup>17</sup>A. Venzie, A. Portoff, W. B. Fowler, M. Stavola, D. W. Jeon, J. Kim, and S. J. Pearton, *Appl. Phys. Lett.* **120**, 192101 (2022).
- <sup>18</sup>A. Y. Polyakov *et al.*, *J. Appl. Phys.* **132**, 035701 (2022).
- <sup>19</sup>A. Sharma and U. Singiseti, *Appl. Phys. Lett.* **118**, 032101 (2021).
- <sup>20</sup>A. Segura, L. Artus, R. Cusco, R. Goldhahn, and M. Feneberg, *Phys. Rev. Mater.* **1**, 024604 (2017).
- <sup>21</sup>M. Hilfiker, R. Korlacki, R. Jinno, Y. Cho, H. G. Xing, D. Jena, U. Kilic, M. Stokey, and M. Schubert, *Appl. Phys. Lett.* **118**, 062103 (2021).
- <sup>22</sup>M. Feneberg, J. Nixdorf, M. D. Neumann, N. Esser, L. Artus, R. Cusco, T. Yamaguchi, and R. Goldhahn, *Phys. Rev. Mater.* **2**, 044601 (2018).
- <sup>23</sup>M. Stokey *et al.*, *Phys. Rev. Mater.* **6**, 014601 (2022).
- <sup>24</sup>S. I. Kan, S. Takemoto, K. Kaneko, I. Takahashi, M. Sugimoto, and T. Shinohe, *Appl. Phys. Lett.* **113**, 212104 (2018).
- <sup>25</sup>J. G. Hao, H. H. Gong, X. H. Chen, Y. Xu, F. F. Ren, and S. L. Gu, *Appl. Phys. Lett.* **118**, 261601 (2021).
- <sup>26</sup>J. P. McCandless *et al.*, *Appl. Phys. Lett.* **119**, 062102 (2021).
- <sup>27</sup>J. G. Hao, H. H. Gong, X. H. Chen, Y. Xu, F.-F. Ren, S. L. Gu, R. Zhang, Y. D. Zheng, and J. D. Ye, *Appl. Phys. Lett.* **118**, 261601 (2021).
- <sup>28</sup>S. I. Kan, S. Takemoto, K. Kaneko, I. Takahashi, M. Sugimoto, T. Shinohe, and S. Fujita, *Appl. Phys. Lett.* **113**, 212104 (2018).
- <sup>29</sup>D. Jung, Y. Jang, P. R. Sultane, C. W. Bielawski, and J. Oh, *J. Alloys Compd.* **922**, 166197 (2022).
- <sup>30</sup>X. Xia, J. S. Li, C. C. Chiang, T. J. Yoo, F. Ren, H. Kim, and S. J. Pearton, *J. Phys. D: Appl. Phys.* **55**, 385105 (2022).
- <sup>31</sup>H. H. Gong, X. H. Chen, Y. Xu, Y. T. Chen, F. F. Ren, B. Liu, S. L. Gu, R. Zhang, and J. D. Ye, *IEEE Trans. Electron Devices* **67**, 3341 (2020).
- <sup>32</sup>S. Ghosh, M. Baral, R. Kamparath, S. D. Singh, and T. Ganguli, *Appl. Phys. Lett.* **115**, 251603 (2019).
- <sup>33</sup>X. Lu, Xianda Zhou, Huaxing Jiang, Kar Wei Ng, Zimin Chen, Yanli Pei, Kei May Lau, and Gang Wang, *IEEE Electron Device Lett.* **41**, 449 (2020).
- <sup>34</sup>J. Zhang *et al.*, *ACS Appl. Electron. Mater.* **2**, 456 (2020).
- <sup>35</sup>H. Son and D.-W. Jeon, *J. Alloy Compd.* **773**, 631 (2019).
- <sup>36</sup>J. A. Spencer, A. L. Mock, A. G. Jacobs, M. Schubert, Y. Zhang, and M. J. Tadjer, *Appl. Phys. Rev.* **9**, 011315 (2022).
- <sup>37</sup>L. Mattheiss, *Phys. Rev. B* **5**, 290 (1972).
- <sup>38</sup>R. Powell and W. Spicer, *Phys. Rev. B* **2**, 2182 (1970).
- <sup>39</sup>B. D. Vezbickie, S. Patel, B. E. Davis, and D. P. Birnie, *Phys. Status Solidi B* **252**, 1700 (2015).
- <sup>40</sup>T. A. Morgan *et al.*, *ACS Appl. Mater. Interfaces* **14**, 33944 (2022).
- <sup>41</sup>E. A. Kraut, R. W. Grant, J. R. Waldrop, and S. P. Kowalczyk, *Phys. Rev. Lett.* **44**, 1620 (1980).
- <sup>42</sup>S. A. Chambers, L. Wang, and D. R. Baer, *J. Vac. Sci. Technol. A* **38**, 061201 (2020).
- <sup>43</sup>G. Greczynski and L. Hultman, *J. Appl. Phys.* **132**, 011101 (2022).
- <sup>44</sup>G. Greczynski and L. Hultman, *Sci. Talks* **1**, 100007 (2022).
- <sup>45</sup>C. Fares, F. Ren, Max Knessl, H. von Wenckstern, M. Grundmann, and S. J. Pearton, "Chapter 9," in *Wide Bandgap Semiconductor Based Electronics*, edited by F. Ren and S. J. Pearton (IOP, Bristol, 2020).
- <sup>46</sup>D. C. Hays, B. P. Gila, S. J. Pearton, and F. Ren, *Appl. Phys. Rev.* **4**, 021301 (2017).
- <sup>47</sup>X. Xia, J.-S. Li, C.-C. Chiang, T. J. Yoo, F. Ren, H. Kim, and S. J. Pearton, *J. Vac. Sci. Technol. A* **40**, 053401 (2022).
- <sup>48</sup>A. Polyakov, V. Nikolaev, S. Stepanov, A. Almaev, A. Pechnikov, E. Yakimov, B. O. Kushnarev, I. Shchemerov, M. Scheglov, A. Chernykh, A. Vasilev, A. Kochkova, L. Guzilova and S. J. Pearton, *J. Phys. D* **55**, 495102 (2022).
- <sup>49</sup>K. Kaneko, S. Fujita, and T. Hitora, *Jpn. J. Appl. Phys.* **57**, 02cb18 (2018).
- <sup>50</sup>K. Kaneko, Y. Masuda, S.-i. Kan, I. Takahashi, Y. Kato, T. Shinohe, and S. Fujita, *Appl. Phys. Lett.* **118**, 102104 (2021).